Supporting Information

Insights into the Recognition, Binding and Reactivity of Catalytic Metallodrugs Targeting Stem Loop IIb of Hepatitis C IRES RNA.

Seth S. Bradford[1+], Martin James Ross[1+], Insiya Fidai[1] and J. A. Cowan[1,2*]

Contribution from [1] Evans Laboratory of Chemistry, The Ohio State University, 100 West 18th Avenue, Columbus, Ohio 43210, and [2] MetalloPharm LLC, 1790 Riverstone Drive, Delaware, OH 43015

RECEIVED DATE (to be automatically inserted after your manuscript is accepted if required according to the journal that you are submitting your paper to)

[+] Authors contributed equally

* Correspondence to: Dr. J. A. Cowan, Evans Laboratory of Chemistry, The Ohio State University, 100 West 18th Avenue, Columbus, Ohio 43210. Tel: 614 292 2703; Fax: 614 292 1685; e-mail: cowan@chemistry.ohio-state.edu

Table SM1. List of new mass spectrometric peaks observed after reaction with **1**-Cu for 60 minutes.

Theoretical Mass	Observed Mass	Mass Error(ppm)	Position	Overhang
1532.05	1531.77	-184.85	3	2,3-cyclic phosphate
1861.26	1861.41	79.06	4	2,3-cyclic phosphate
2206.47	2206.80	151.26	5	2,3-cyclic phosphate
2535.68	2536.00	127.96	6	2,3-cyclic phosphate
2864.89	2865.43	187.78	7	2,3-cyclic phosphate
3539.31	3539.89	164.81	9	2,3-cyclic phosphate
3844.49	3845.06	147.98	10	2,3-cyclic phosphate
4189.70	4190.35	155.97	11	2,3-cyclic phosphate
4495.87	4496.30	95.04	12	2,3-cyclic phosphate
4801.05	4801.55	104.43	13	2,3-cyclic phosphate
5107.22	5107.76	106.53	14	2,3-cyclic phosphate
5436.43	5436.78	64.51	15	2,3-cyclic phosphate
5781.64	5782.25	105.32	16	2,3-cyclic phosphate
6086.82	6087.06	38.81	17	2,3-cyclic phosphate
6392.00	6392.28	43.17	18	2,3-cyclic phosphate
7027.38	7027.40	3.55	20	2,3-cyclic phosphate
11184.93	11184.49	-39.18	33	3'-OH
2553.70	2553.83	52.65	6	3'-phosphate
2882.91	2883.71	277.75	7	3'-phosphate
3212.12	3213.05	290.24	8	3'-phosphate
6410.02	6411.63	251.43	18	3'-phosphate
6381.85	6380.98	-136.23	15	5'-OH
6052.64	6051.91	-121.23	16	5'-OH
5707.43	5706.91	-91.83	17	5'-OH
5402.25	5401.74	-93.57	18	5'-OH
5097.07	5096.66	-79.87	19	5'-OH
4767.86	4767.04	-171.87	20	5'-OH

4461.69	4461.19	-112.29	21	5'-OH
4116.48	4116.24	-58.56	22	5'-OH
3771.27	3771.03	-64.69	23	5'-OH
3466.09	3465.79	-87.16	24	5'-OH
3120.88	3120.57	-99.56	25	5'-OH
2814.71	2814.47	-84.71	26	5'-OH
2508.54	2508.59	18.73	27	5'-OH
2179.33	2179.15	-82.42	28	5'-OH
1834.12	1833.88	-132.13	29	5'-OH
1527.95	1528.00	30.82	30	5'-OH
2588.52	2588.00	-201.31	27	5'-phosphate

Table SM2. List of mass spectrometric peaks observed after reaction with **2**-Cu for 60 minutes.

Theoretical Mass	Observed Mass	Mass Error(ppm)	Position	Overhang
1861.26	1861.51	134.05	4	2,3-cyclic phosphate
2206.47	2206.75	124.77	5	2,3-cyclic phosphate
2864.89	2865.19	105.16	7	2,3-cyclic phosphate
3194.10	3194.54	139.08	8	2,3-cyclic phosphate
3539.31	3539.69	107.64	9	2,3-cyclic phosphate
3844.49	3844.76	70.23	10	2,3-cyclic phosphate
4801.05	4801.16	22.46	13	2,3-cyclic phosphate
5107.22	5107.34	22.86	14	2,3-cyclic phosphate
5436.43	5435.94	-90.75	15	2,3-cyclic phosphate
6392.00	6391.74	-40.35	18	2,3-cyclic phosphate
1550.07	1550.00	-43.19	3	3'-phosphate
1879.28	1879.77	262.35	4	3'-phosphate
2553.70	2553.43	-105.85	6	3'-phosphate
5097.07	5096.66	-81.20	19	5'-OH
4461.69	4461.50	-41.83	21	5'-OH
4116.48	4116.50	5.05	22	5'-OH
3771.27	3771.30	8.18	23	5'-OH
3466.09	3465.98	-32.93	24	5'-OH
2814.71	2814.68	-10.84	26	5'-OH
2508.54	2508.64	38.22	27	5'-OH
2179.33	2179.36	11.80	28	5'-OH
1834.12	1833.79	-179.99	29	5'-OH
1527.95	1527.89	-37.27	30	5'-OH
1914.10	1914.42	164.90	29	5'-phosphate
1607.93	1607.94	6.45	30	5'-phosphate

Table SM3. Subcluster assignments of **1**-Cu based on proximity of the copper atom to the site of reactivity as determined by mass spectrometry.

Pose	Atom	RNA Residue	RNA Atom	Distance Å	Assigned Cluster
2	Cu	U12	OP1	1.4	U14
6	Cu	C13	OP1	1.5	U14
7	Cu	U12	OP2	2.2	U14
11	Cu	U12	OP1	1.6	U14
15	Cu	U12	OP1	1.6	U14
16	Cu	U12	OP2	4	U14
19	Cu	C13	OP2	1.6	U14
26	Cu	U14	O4	2.3	U14
27	Cu	C13	OP2	3.7	U14
32	Cu	C13	OP1	2.9	U14
33	Cu	U14	OP2	1.7	U14
35	Cu	C13	OP2	1.6	U14
36	Cu	U12	OP2	4.2	U14
37	Cu	C13	OP2	1.7	U14
39	Cu	U14	O4	2.8	U14
44	Cu	U14	OP2	4.3	U14
10	Cu	C18	OP1	1.4	C18
25	Cu	C18	OP1	4.2	C18
31	Cu	C18	OP1	1.7	C18
38	Cu	C18	OP1	1.6	C18
45	Cu	G16	OP2	6.4	C18
1	Cu	A19	OP2	1.7	A19
17	Cu	A19	OP2	4.4	A19
22	Cu	A19	OP2	3.2	A19
23	Cu	A19	OP2	4.1	A19
28	Cu	A19	OP2	4.2	A19
29	Cu	A19	OP2	8	A19
40	Cu	A19	OP2	5.5	A19
42	Cu	A19	OP2	3.1	A19
43	Cu	A19	OP2	3.5	A19
3	Cu	C10	OP2	1.5	G21
4	Cu	U20	OP2	3.4	G21
5	Cu	U20	OP2	1.7	G21
8	Cu	C10	OP2	1.9	G21
9	Cu	U20	OP2	1.6	G21
12	Cu	G9	OP2	2.3	G21

13	Cu	C10	OP2	1.5	G21
18	Cu	C10	OP1	2.9	G21
20	Cu	C10	OP1	2	G21
21	Cu	G9	OP1	1.6	G21
24	Cu	G11	OP1	1.7	G21
30	Cu	U20	OP2	1.8	G21
34	Cu	C10	OP2	1.7	G21
36	Cu	U12	OP2	4.2	G21
41	Cu	U20	OP2	1.6	G21

Table SM4. Subcluster assignments of **2**-Cu based on proximity of the copper atom to the site of reactivity as determined by mass spectrometry.

Pose	Atom	RNA Residue	RNA Atom	Distance Å	Assigned Cluster
25	Cu	A6	OP1	3.8	A6
27	Cu	A6	OP1	2.8	A6
29	Cu	A6	OP1	4.8	A6
33	Cu	A6	HO2'	2.7	A6
76	Cu	A6	OP1	3.6	A6
87	Cu	A6	OP2	4.2	A6
14	Cu	A7	OP1	3.5	A7
17	Cu	A7	OP1	1.7	A7
22	Cu	A7	OP1	1.4	A7
30	Cu	A7	OP1	1.7	A7
34	Cu	A7	OP1	2.6	A7
38	Cu	A7	OP1	2.1	A7
39	Cu	A7	OP1	1.3	A7
40	Cu	A7	OP1	1.6	A7
42	Cu	A7	OP1	4.5	A7
43	Cu	A7	OP1	1.6	A7
50	Cu	A7	OP1	1.7	A7
59	Cu	A7	OP1	1.6	A7
74	Cu	A7	OP2	4	A7
78	Cu	A7	OP1	2.8	A7
1	Cu	A8	OP1	1.5	A8
3	Cu	A8	OP1	2.4	A8
5	Cu	A8	OP1	1.7	A8
6	Cu	A8	OP1	1.6	A8
7	Cu	A8	OP1	4.7	A8
8	Cu	A8	OP1	3.4	A8
10	Cu	A8	OP1	1.6	A8
16	Cu	A8	OP1	1.5	A8
19	Cu	A8	OP1	1.7	A8
20	Cu	A8	OP1	1.5	A8
24	Cu	A8	OP1	2.2	A8
32	Cu	A8	OP1	2	A8
35	Cu	A8	OP1	1.5	A8
36	Cu	A8	OP1	1.6	A8
41	Cu	A8	OP1	3.1	A8
51	Cu	A8	OP1	1.5	A8

53	Cu	A8	OP1	1.8	A8
55	Cu	A8	OP1	1.5	A8
57	Cu	A8	OP2	4.4	A8
60	Cu	A8	OP1	3.1	A8
62	Cu	A8	OP1	1.9	A8
66	Cu	A8	OP1	4.9	A8
69	Cu	A8	OP1	5	A8
72	Cu	A8	OP1	1.6	A8
77	Cu	A8	OP2	3.7	A8
82	Cu	A8	OP2	3.2	A8
83	Cu	A8	OP1	1.5	A8
9	Cu	C23	OP2	3.7	C23
15	Cu	C23	OP2	2.6	C23
61	Cu	C23	OP2	4.1	C23
64	Cu	C23	OP1	6.6	C23
68	Cu	C23	OP2	3.6	C23
73	Cu	C23	OP2	4.1	C23
85	Cu	C23	OP2	2.5	C23
86	Cu	C23	OP2	4	C23
2	Cu	G22	OP1	1.6	G22
21	Cu	G22	OP2	3.3	G22
31	Cu	G22	OP2	3.8	G22
37	Cu	G22	OP2	1.7	G22
44	Cu	G22	OP1	3.6	G22
46	Cu	G22	OP1	3.8	G22
47	Cu	G22	OP2	1.7	G22
48	Cu	G22	OP1	1.5	G22
52	Cu	G22	OP2	1.7	G22
54	Cu	G22	OP1	3.6	G22
67	Cu	G22	OP2	2.3	G22
71	Cu	G22	OP2	4.2	G22
81	Cu	G22	OP1	4.4	G22
84	Cu	G22	OP1	1.4	G22
88	Cu	G22	OP1	2.6	G22

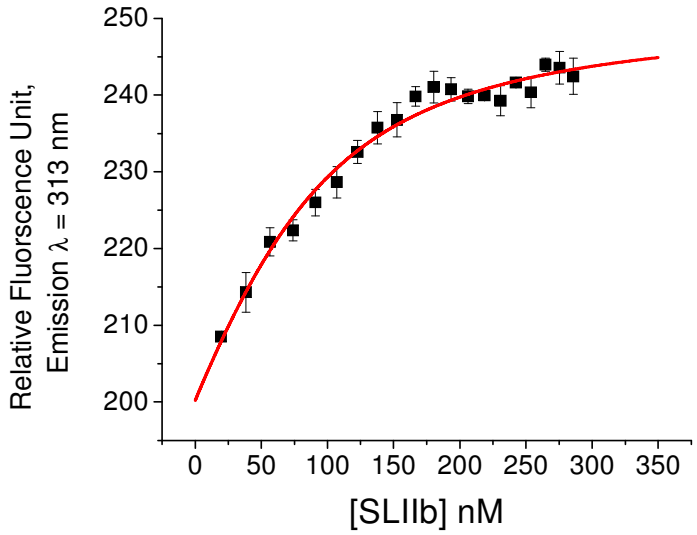

Figure SM1. The determination of K_D for **2** via changes in tyrosine fluorescence. K_D = 76 nM ± 3 nM. [**2**-Cu] = 84 nM , [HEPES] = 20 mM, [NaCl] = 100 mM, pH = 7.4.

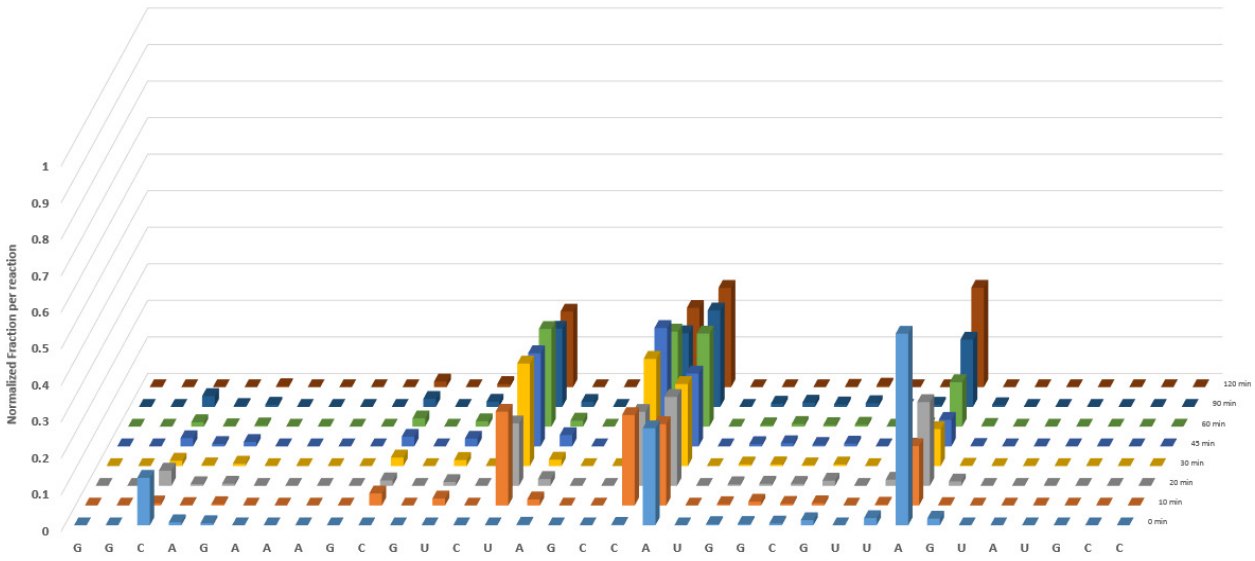

Figure SM2. Summary of cleavage sites on SLIIb RNA promoted by **1**-Cu as determined by mass spectrometric measurements. The plot shows the formation of products at each position as a function of time following reaction with **1**-**Cu** in the presence of co-reagents. Reaction sites are defined as those with products at six or more time points.

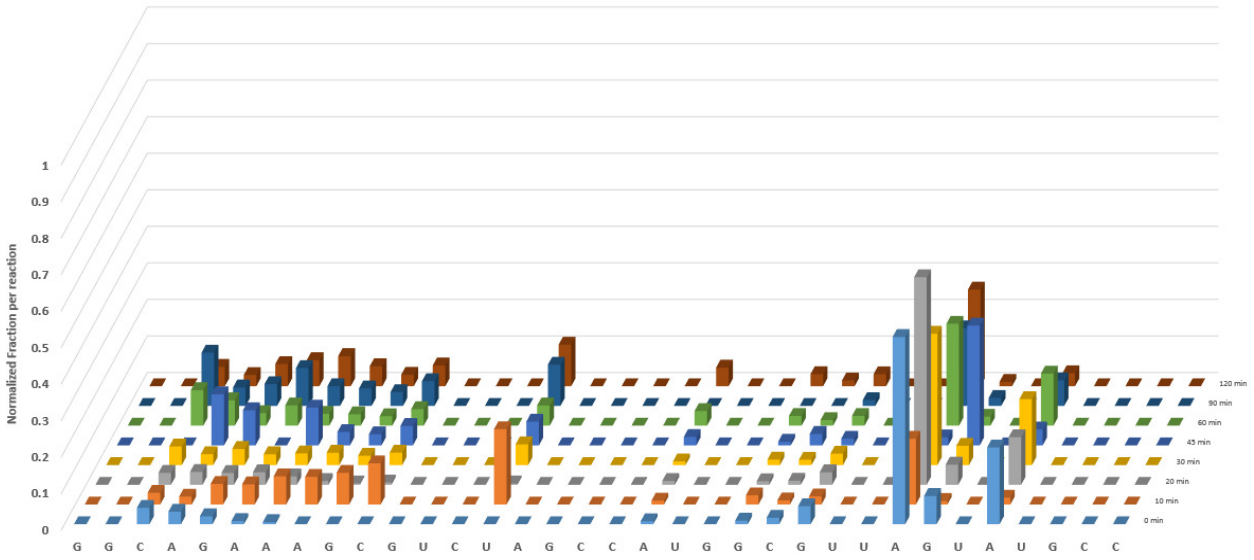

Figure SM3. Summary of cleavage sites on SLIIb RNA promoted by **2**-Cu as determined by spectrometric measurements. The plot shows the formation of products at each position as a function of time following reaction with **2**-**Cu** in the presence of co-reagents. Reaction sites are defined as those with products at six or more time points.

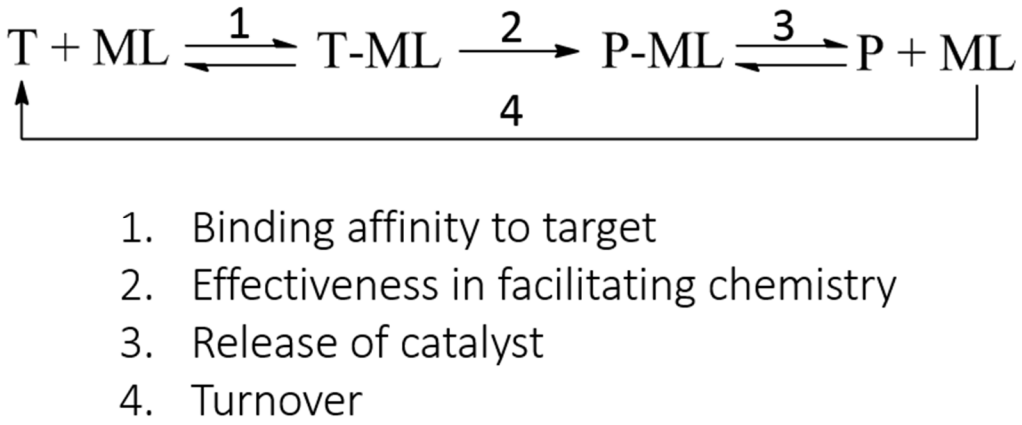

Figure SM4. A summary of the properties expected to contribute to and influence the effectiveness of catalytic metallodrugs. Unlike traditional drugs, the binding affinity to the target is only one of the factors that influence the effectiveness of the catalytic drug. Further, there needs to be a balance between the affinity to the target and the release of the therapeutic agent from the modified target.

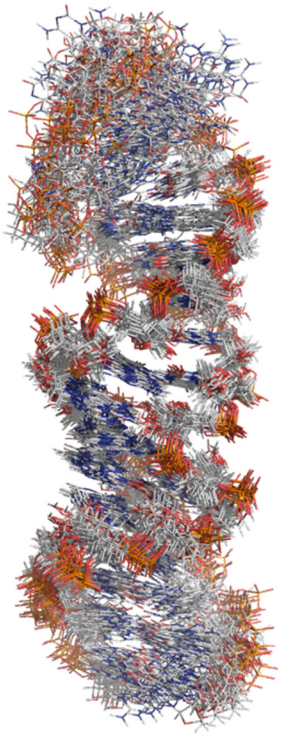

Figure SM5. Overlap of the 20 NMR structures available in the PDB file 1P5N. The top of the RNA is the most dynamic portion of stem loop IIb, while the rest is more rigid.

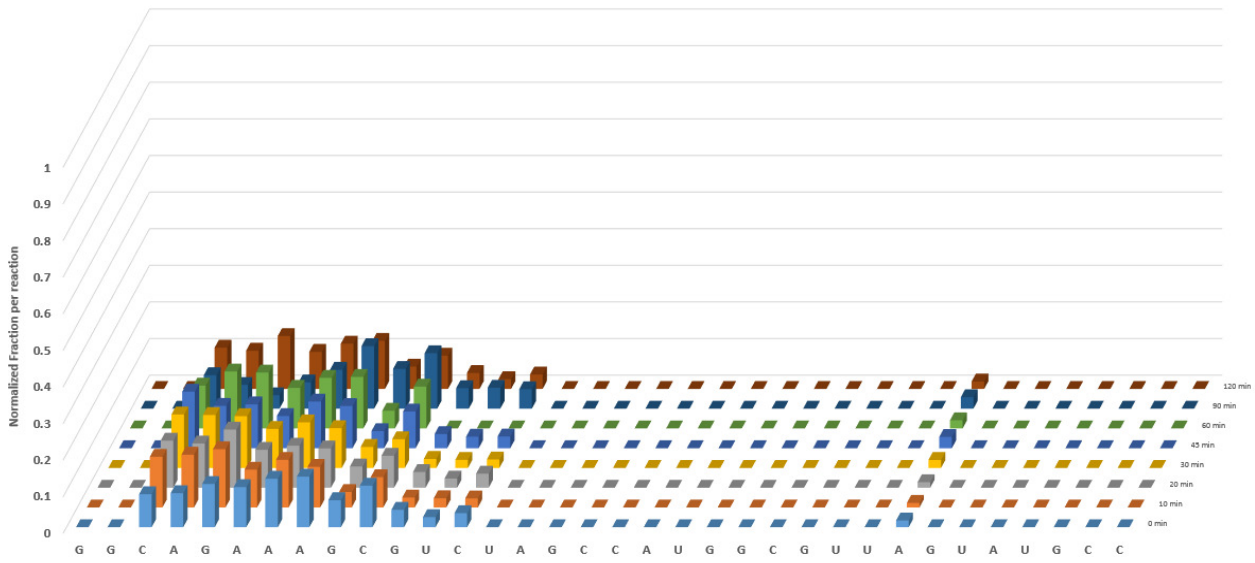

Figure SM6. Summary of cleavage sites on SLIIb RNA by **1**-Cu as determined by mass spectrometry, showing the formation of products at each position as a function of time following reaction mediated by catalyst in the absence of co-reagents. Reaction sites are those with products at six or more time points.

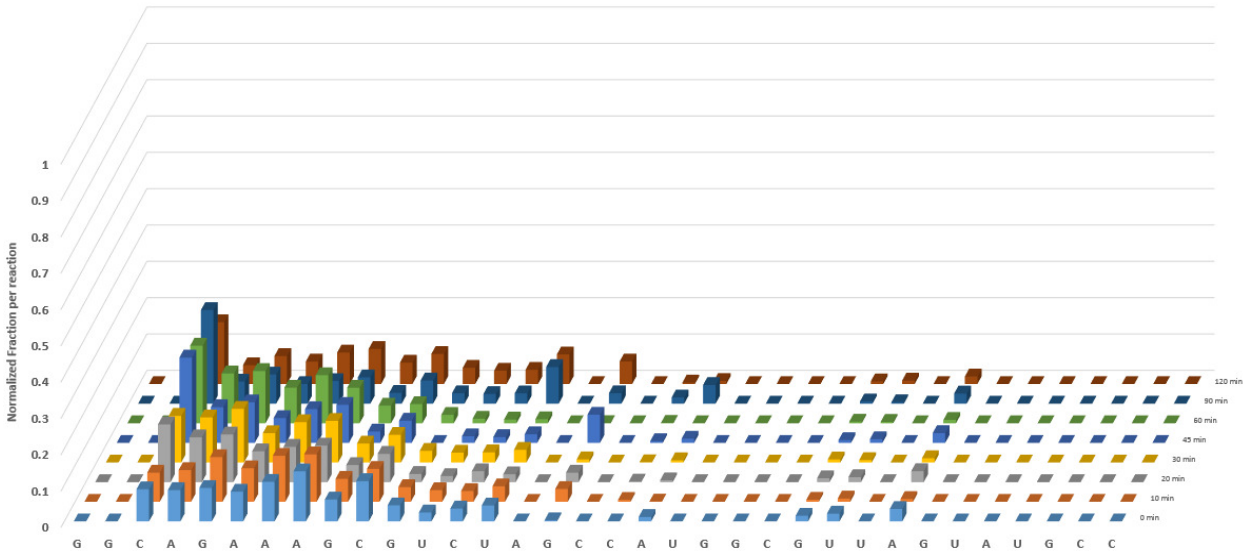

Figure SM7. Summary of cleavage sites on SLIIb RNA by **2**-Cu as determined by mass spectrometry, showing the formation of products at each position as a function of time following reaction mediated by catalyst in the absence of co-reagents. Reaction sites are those with products at six or more time points.

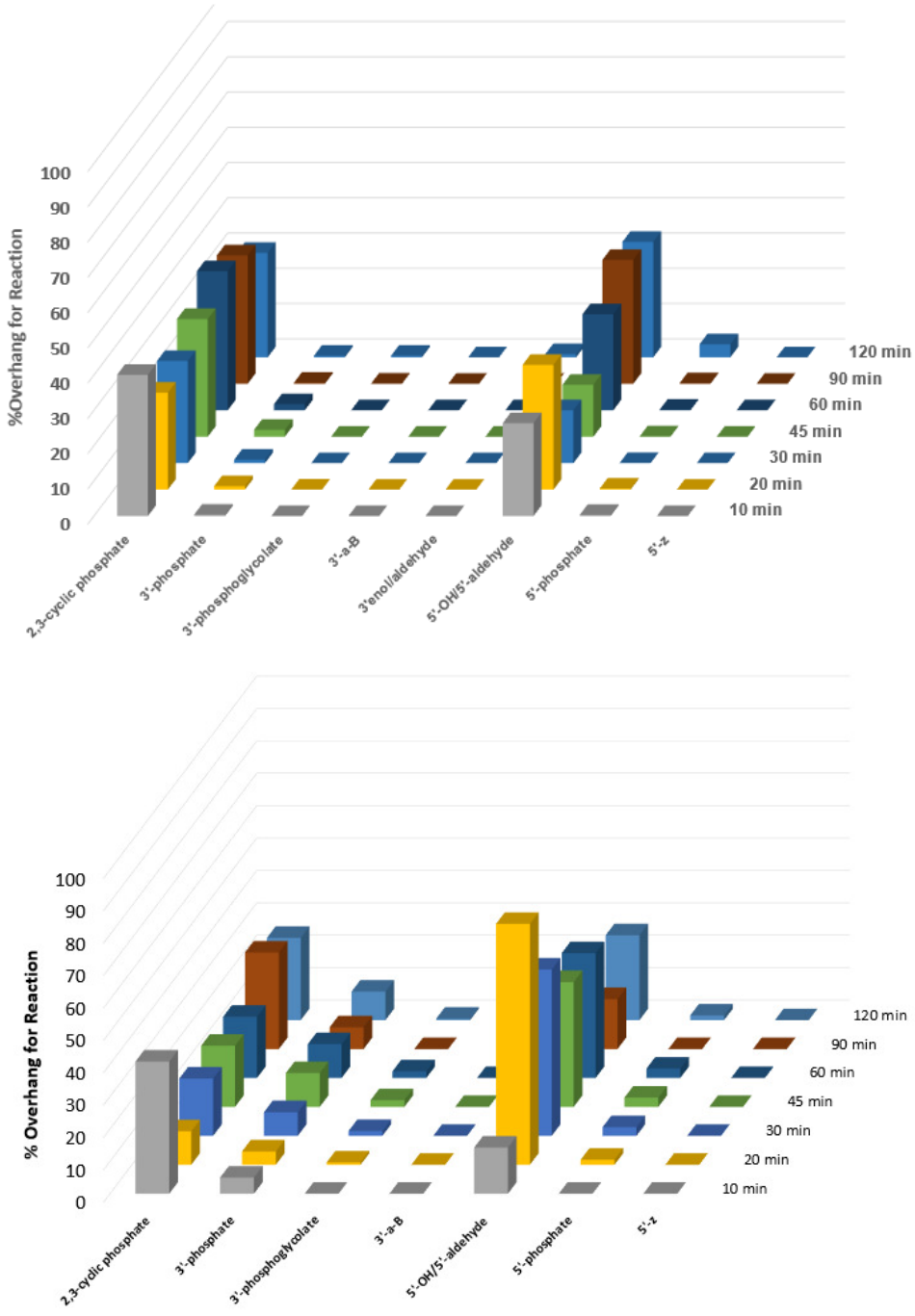

Figure SM8. Relative amounts of each class of product observed by mass spectrometry displayed as a function of time following reaction with **1**-Cu (top) and **2**-Cu (bottom). **1**-Cu produced almost exclusively 2',3'-cyclic phosphates for the 3'-overhang whereas for **2**-Cu the relative amounts were about two-thirds 2',3'-cyclic phosphates and one-third 3'-phosphates.

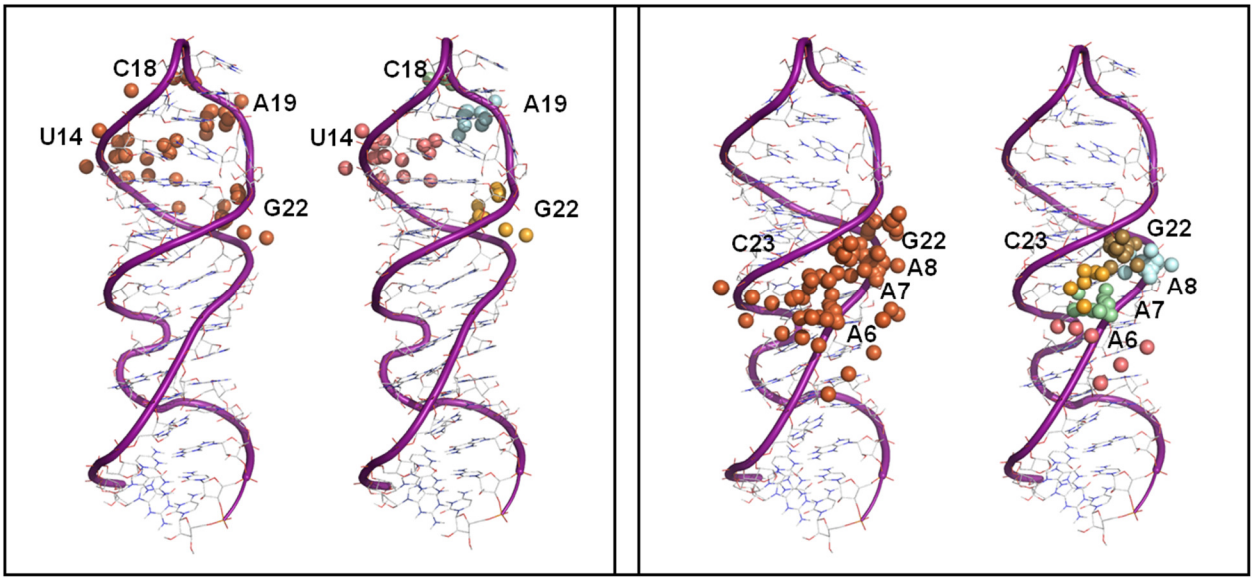

Figure SM9. (Colored variant of Figure 6). The metal ion, shown as a sphere, for each bound metallopeptide conformer from docking to the top conformation of the NMR structure of SLIIb in Autodock. (Left box, left image) Positions of the docked metal ion for each conformation of the RNA-complexed metallopeptide **1**-Cu. (Left box, right image) The subclusters of metal ions distributed around bases (individually color-coded) which correspond to experimentally observed sites of reaction for 1-Cu (pink, U14; green C18; blue, A19; yellow, G22). (Right box, left image) Positions of the docked metal ion for each conformation of the RNA-complexed metallopeptide **2**-Cu. (Right box, right image) The subclusters of metal ions distributed around bases which correspond to experimentally observed sites of reaction for 2-Cu (pink, A6; green A7; blue A8; yellow, C23; brown, G22).

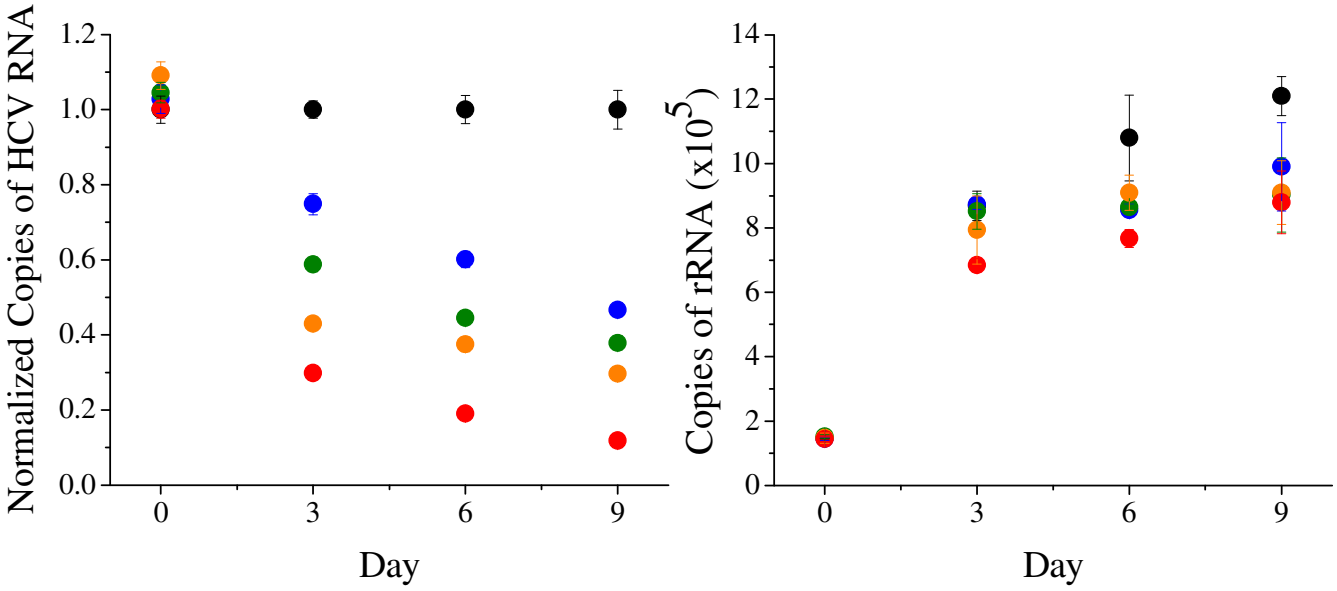

Figure SM10. (Colored variant for Figure 7). RT-PCR results showing the preferential cleavage of HCV RNA (left) over ribosomal RNA (right) at increasing dosages of **1**-Cu. 0 μM (black), 2.5 μM (blue), 5 μM (green), 10 μM (orange), 20 μM (red). The graph on the left is normalized to the RNA levels in the absence of metallopeptide.

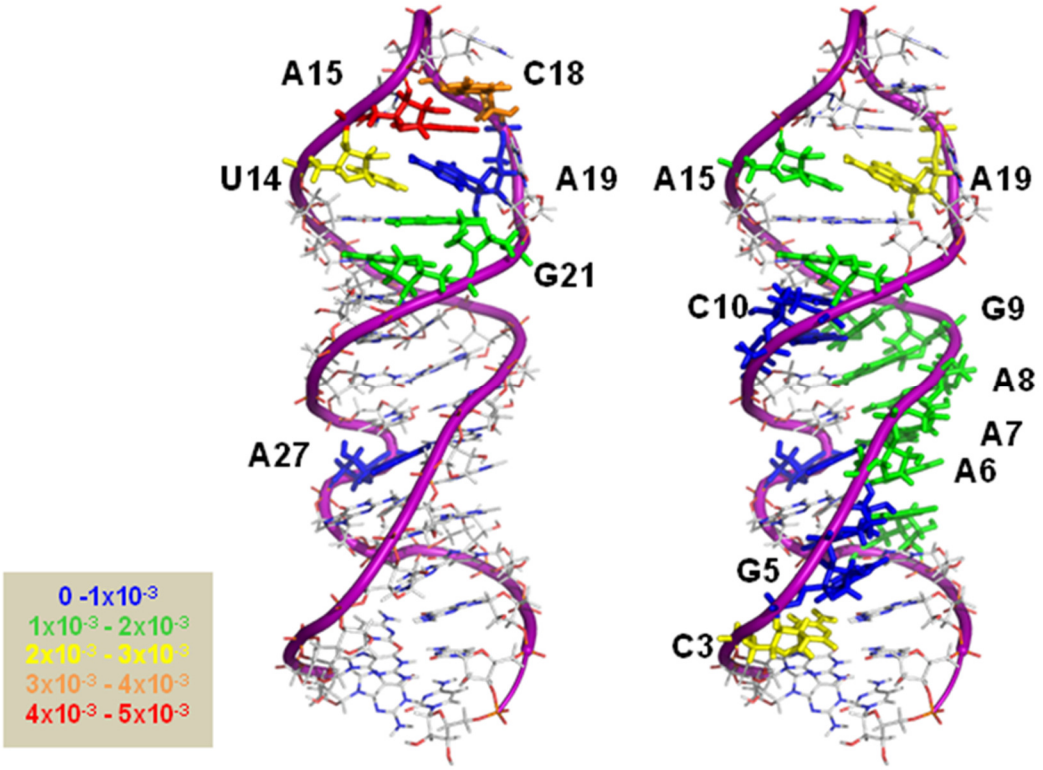

Figure SM11. (Colored variant for Figure 8). Sites of reactivity based on MALDI assignments of fragments that show a time dependence in the presence of **1**-Cu with SLIIb (left) and **2**-Cu with SLIIb (right). The scale reflects the relative initial velocity for reaction at each position with time (per minute) as described in the experimental section.

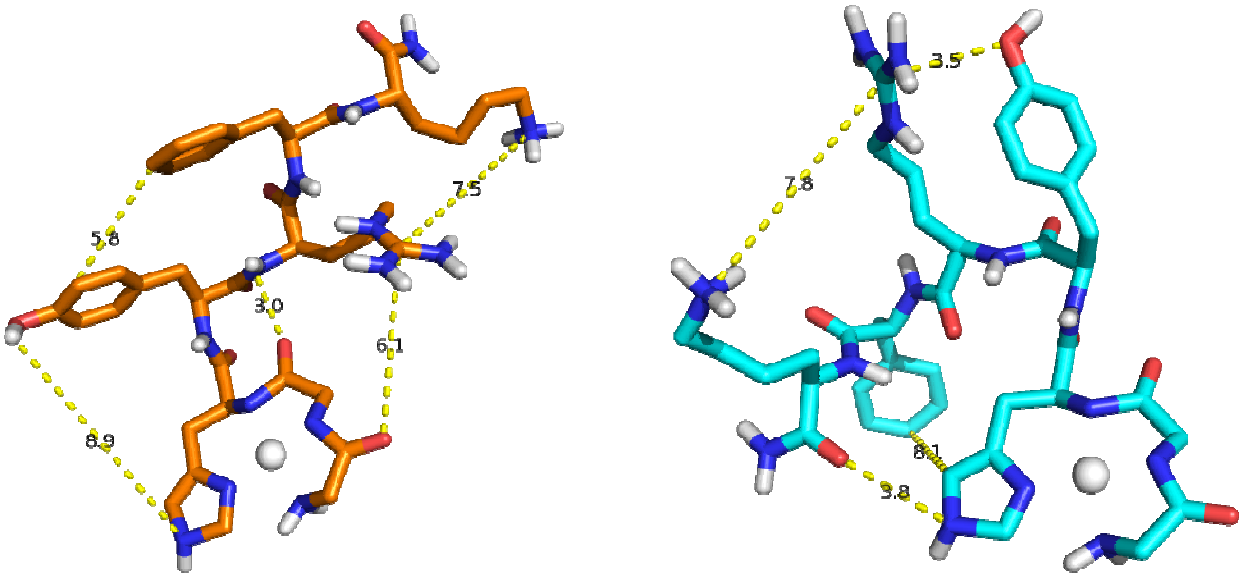

Figure SM12. The optimized solution structures of Cu-GGHYrFK-amide (left) and Cu-GGhyrfk-amide (right). Distances are shown in Angstroms. Structures were optimized in Gaussian and images were produced in PyMol.

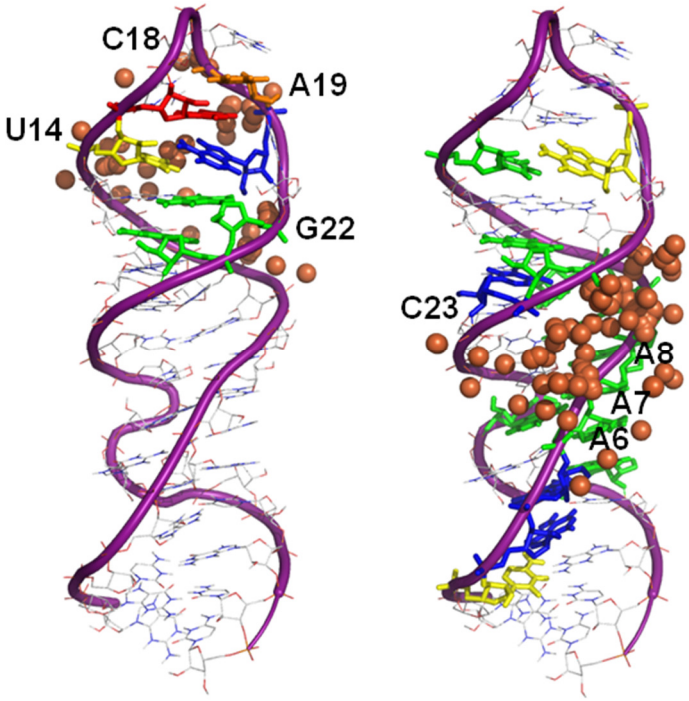

Figure SM13. (Colored variant for Figure 11). Comparison of the reactive sites based upon the MALDI-TOF MS, the colored residues, (Figure SM11) overlaid with the simulated binding proposed by Autodock, orange spheres represent copper atoms, (Figure SM9) for **1**-Cu (left), and **2**-Cu (right).